NEAR REAL-TIME DEFORMATION MONITORING BASED ON PERSISTENT SCATTERER INTERFEROMETRY

Ling Chang[(1)], Ramon F. Hanssen[(1)]

(1) Delft University of Technology, Kluyverweg 1, 2629 HS Delft, The Netherlands,

Email: L.Chang@tudelft.nl, R.F.Hanssen@tudelft.nl

ABSTRACT

In this paper, we present a complete procedure for Near Real-time (NRT) deformation monitoring by Persistent Scatterer Interferometry (PSI). Frequent-update short-time interferograms are used. Persistent scatterers are long-term stable, but not necessarily over the full time series. In this study, the key focus is to identify and characterize all available points and to track their deformation time series. Moreover, a robust testing approach is performed to discriminate between reliable deformation of points and errors induced by noise.

To evaluate the algorithm, we carry out a case study over Delft, the Netherlands. Sixty descending TerraSAR-X images acquired between April 2009 and April 2011 are studied. From this experiment, the feasibility of NRT deformation monitoring can be demonstrated, as well as the reliability of the deformation time series for all tracked points. Meanwhile, it provides an alarm when the deformation behavior is anomalous, to enable mitigating actions.

KEY WORDS: Near Real-time deformation monitoring; TerraSAR-X

1. INTRODUCTION

Persistent Scatterer Interferometry (PSI) builds a convenient processing framework that enables the use of all acquired images, irrespective of baseline, and a parameter estimation strategy for interferograms with low spatial coherence, [1, 4]. Its aim is to bypass the spatial and temporal decorrelation by considering time-coherent pixels [2]. By using a large amount (typically more than 20) of images, the atmospheric phase component is estimated and corrected for. This technique has been successfully applied to different cases from surface deformation monitoring to natural disaster monitoring. In terms of various particular cases, advanced PSI techniques and their application have been proposed, see e.g. Ferretti et al. [3], Marinkovic et al. [4], Marek Mrz [8], Hooper [11].

PSI has the capability to study the past by exploring data archives at once in a stack of images, generally. Once the new acquisition yields new data, the whole processing is required again, which leads to the disappearance of parts of the PS points due to decreased coherence. It is obvious that the main drawback of the PSI technique is the limited spatial density of targets that behave coherently during the whole observation span [7]. Obviously, the lack of obtained PS points in an area of interest would prevent deformation monitoring.

This paper is focused on Near Real-time (NRT) deformation monitoring in urban areas by means of PSI, which adds new acquisition data to an existing stack, updates the sequential estimation of parameters, identifies and characterizes all available PS points and tracks their deformation time history. Moreover, according to the prior adapted deformation model of each point and their spatial distribution of deformation behavior, a robust testing approach is designed to discriminate between the deformation of points and errors induced by noise. We will show the results obtained by performing such approach in the study area of Delft, the Netherlands, with TerraSAR-X StripMap mode data.

2. NEAR REAL-TIME PSI TECHNIQUES DEFINITATION

2.1 Near Real-time PSI Processing System

The Near Real-time (NRT) PSI processing system depends on the PSI techniques with frequent-update data. Thanks to the increasing amount of high resolution TerraSAR-X SAR images with short time intervals, such NRT PSI processing system has been feasible, as proposed by Marinkovic et al [4]. This section presents a NRT PSI processing system that tracks the deformation behavior of all PS points, classifies them on specific characteristics, and performs rigorous testing to discriminate actual PS deformation from noise. It provides an alarm when the deformation behavior is anomalous, to enable mitigating actions.

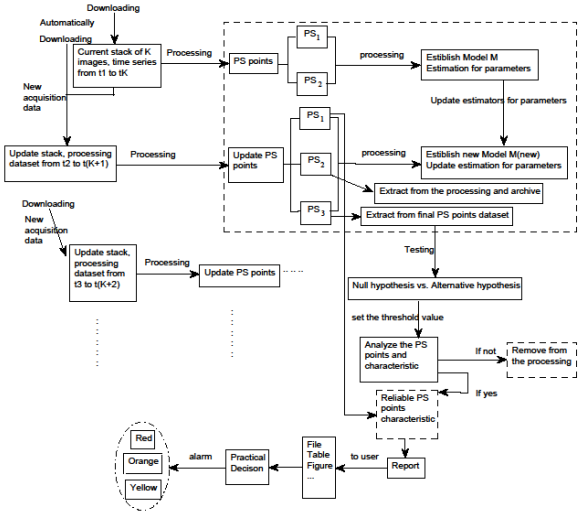

Figure 1. The flowchart for the NRT PSI processing system

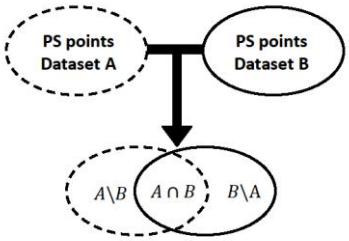

Figure 2. The Venn diagram for the relationship of PS datasets from two processing datasets

As shown in Fig. 1, the NRT PSI processing system consists of four steps: 1) check for the new data and download automatically. 2) process the dataset where a new data are introduced, obtain the PS points with their deformation behavior, and classify PS points into three classes. Class1 holds the PS points that maintain coherence (PS_1, survivor); Class2 contains the PS points that disappeared (PS_2, extinct) by the new dataset, and the Class3 contains the potentially new-born PS points (PS_3, new). The Venn diagram in Fig. 2 illustrates the logical relationship of PS datasets from two processing datasets. It is straightforward to find out that the PS points in intersection part of datasets A and B are from Class1. The PS points in the complementary parts belong to Class2 and Class3. 3) considering the different behavior between these three classes of PS points, the extinct PS_2 points are extracted for individual further testing. After removing the unreliable scatterers according to the testing approach, deformation information for all available points is collected. 4) report on the deformation behavior of PS points, and assist the user to give an alarm for abnormal deformation for certain targets (i.e. buildings, bridges). In future the alarm flag with Red/Orange/Yellow will denote the corresponding location of the targets on the map.

2.2 The Classification Criteria for Three Classes PS Points

As mentioned in previous section, the PS points can be divided into three classes in terms of their stability. Let us define a square $n \times n$ matrix M, where n is the number of frequent-updated dataset. The elements $M_{i,i}$ $(i = 1 \ldots n)$ on the diagonal are the ``storage box`` for surviving PS points which are stable through the time series (PS_1). Each element $M_{i,j} (i < j = 2 \ldots n)$ on the lower triangular off-diagonal are the ``storage box`` for the extinct PS points (PS_2) which disappear when new data adds in. The more difference between i and j, the more PS points which belong to the previous dataset will become extinct. Practically, some PS points could reappear in further processing. On the other hand, the elements $M_{i,j} (i > j = 1 \ldots n)$ on the upper triangular off-diagonal are the ``storage box`` for new PS points (PS_3). The explanatory matrix which shows the relationship matrix for the PS points from different processing datasets, is defined as:

$$M_{n \times n} = \begin{bmatrix} A & A \setminus B & \cdots & A \setminus Z \\ B \setminus A & B & \cdots & B \setminus Z \\ \vdots & \vdots & \ddots & \vdots \\ Z \setminus A & Z \setminus B & \cdots & Z \end{bmatrix} \quad (1)$$

where $\begin{cases} A = \forall PS_{\tau_A}, \quad \tau_A = [t_1 \quad t_K] \\ B = \forall PS_{\tau_B}, \quad \tau_B = [t_2 \quad t_{K+1}] \\ \vdots \\ Z = \forall PS_{\tau_Z}, \quad \tau_Z = [t_{n-K+1} \quad t_n] \end{cases}, \quad K \in [2, \quad n]$

and $A \setminus B = \{ PS \in A \mid PS \notin B \}$

Each set has its individual sub-region and may have intersection with others. Here we also address the elements $M_{i,j} (j = i+1, i = 1 \ldots n)$. And hence each PS dataset belongs to this upper triangular off-diagonal elements are extracted and archived. Then it will compare with the further new PS points datasets that are in the lower triangular matrix elements, in order to explore the useful deformation behavior for these partially coherent PS points.

2.3 A Robust Testing Approach and an Adaptive Estimation: the Reliability Evaluation of the Results

The general quality criteria for the selection of PS are temporal ensemble coherence and a-posteriori variance factor are respectively defined as:

$$\hat{\gamma}_{x,y} = \frac{1}{n}\left|\sum_{i=1}^{n}\exp(j\hat{e}_{x,y,i})\right| \quad (2)$$

$$\hat{\sigma}^2 = \frac{\hat{e}^T Q_\phi^{-1}\hat{e}}{r} \quad (3)$$

where j is the imaginary unit, n is the total number of interferograms, $\hat{e}_{x,y,i}$ is the difference between observations and modeled DD phase between points x and y in interferogram i. $\hat{e}$ is the vector of residuals between the unwrapped phase and the deformation model, Q_ϕ is the phase dispersion and r is the redundancy in the functional model.

The PS candidates which have larger $\hat{\gamma}$ and smaller $\hat{\sigma}^2$ than certain two thresholds respectively, are accepted as PS points. However, the results for final PS points are contaminated by type-I errors and type-II errors.

On one hand, type-I errors induce some PS candidates with large $\hat{\sigma}^2$ to be falsely rejected as final PS points. The possible causes for this error are the inappropriate functional model (i.e. the imperfect deformation models), poor specification of the observables' noise characteristics in the stochastic model and observation errors. These PS points should thus be extracted individually and tested by particular alternative hypothesis. The traditional deformation model is linear deformation with only one parameter, described as:

$$a(t) = \frac{-4\pi}{\lambda}\cdot v_{LOS}\cdot t \quad (4)$$

where $a(t)$ is linear deformation model as a function of temporal baseline t, λ is the radar wavelength, and v_{LOS} is a constant deformation velocity in the line of sight (LOS) direction. The linear deformation model has adequate performance in most condition. For a minority of PS points, the adaptive deformation models are required based on hypothesis testing. The observation values might better fit with, e.g. a breakpoint model, a higher order polynomial model or a periodic deformation modal. Here, our testing approach is simply performed by subsequent comparison of two hypotheses: the null hypothesis H_0 and the alternative hypothesis H_A [6]. It can be formed as follows,

$$H_0 : E\{\underline{a}\} = \frac{-4\pi}{\lambda}\cdot v_{LOS}\cdot\begin{bmatrix}t_1 & t_2 & \cdots & t_n\end{bmatrix}^T \quad (5)$$

$$H_A : E\{\underline{a}\} = \frac{-4\pi}{\lambda}\cdot v_{LOS}\cdot\begin{bmatrix}t_1 & t_2 & \cdots & t_n\end{bmatrix}^T + C_a\nabla, \nabla \neq 0 \quad (6)$$

Once the null hypothesis is rejected in terms of a certain critical value k_α, the sequential testing will be performed to search a suitable deformation model.

On the other hand, the final PS point sets might also contain pixels which show good coherence (or low variance) by mere chance. These pixels are caused by type-II errors. They are commonly isolated points which do not have consistent phase behavior in comparison with their neighboring PS points. In order to detect type-II errors, the Spatial-temporal consistency (STC) algorithm, is introduced as a quality assessment for the final selection of PS. The STC of PS points is obtained by comparing its behavior with nearby PS points both in time and space. Hence, the spatial-temporal consistency is defined as:

$$\rho = \min_{\forall p}\frac{\lambda}{4\pi}\sqrt{\frac{1}{n-1}\sum_{i=1}^{n}((\phi_{R,i}-\phi_{P,i})-(\phi_{R,i+1}-\phi_{P,i+1}))^2} \quad (7)$$

where P is the neighboring PS points around the PS point R under consideration. n is the number interferogram, and ϕ is the unwrapped phase in the time series. The advantage of using the STC is that it can reduce the dependency of the PS quality assessment to the assumed deformation model and therefore it is a better indicator for the observations precision. As the new data adds in, the STC threshold for each dataset is adjusted based on STC histogram distribution.

The purpose of all these testing methods above is to acquire the reliable deformation time series for all tracked PS points.

3. EXPERIMENT AND RESULTS

3.1 Data and Study Area Description

TerraSAR-X is the first German radar satellite, launched on June 15th, 2007. The spacecraft acquires high-quality X band radar images of the entire planet while circling earth in a polar orbit at 513km altitude mode with a revisiting time of 11 days. It is able to deliver StripMap mode images with a resolution of up to 3m. We have used a series of StripMap mode (all product type is Single Look Slant Range Complex and in HH polarization mode, descending-pass data) images covering Delft area to study NRT deformation monitoring based on PSI processing (see Fig. 3 that depicted the TerraSAR-X data track 048 coverage and study area). Delft is a city in the province of South

Holland, the Netherlands, and the elevation in part of this flat area is below sea level. Because of its special topographic condition and ongoing infrastructure construction, infrastructure deformation monitoring is indispensable in case of abnormal large deformation.

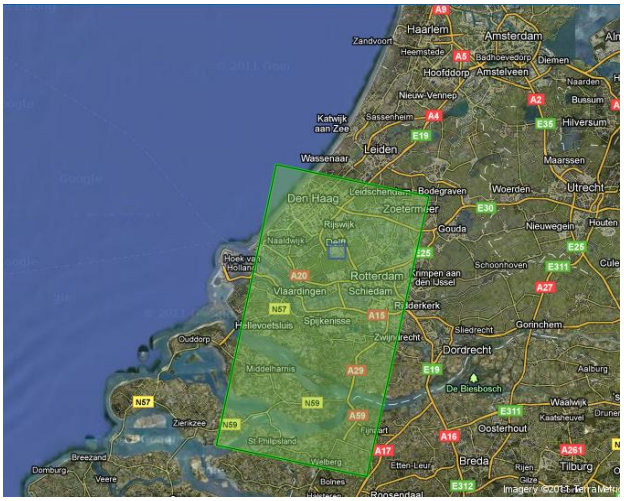

Figure 3. The TerraSAR-X data coverage in green rectangle and the location of study area in blue rectangle

3.2 PSI Processing and Analysis

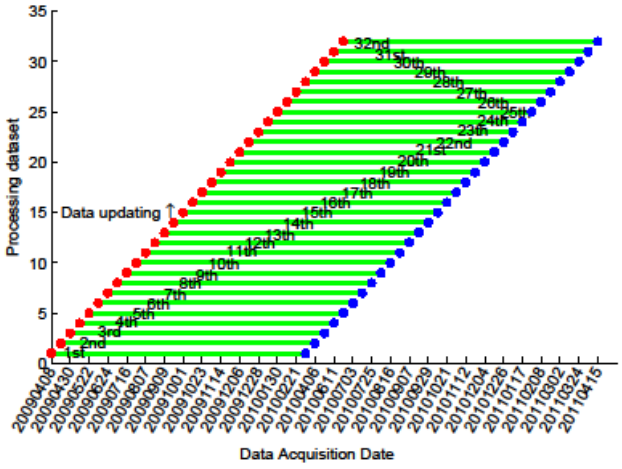

Figure 4. Graph for processing datasets. Each green line represents the time range that starts from the acquisition date with the red dot and ends at the date with the blue dot. The black number on the green line is the number of processing dataset

For the PSI processing, the TU Delft implementation for PS analysis was used. Doris was used for interferograms generation during PSI processing. These sixty SAR image data were acquired from 08th April, 2009 to 15th April, 2011. All the SAR images were cropped in an area of 2.1*km* by 2.1*km*, covering Delft, the Netherlands. All of them were oversampled by a factor of 2 prior to fifty-nine interferograms generation.

In an attempt to simulate the Near Real-time PSI processing, we assumed each dataset was acquired sequentially and PSI processing was performed once the available new-data was obtained. According to the NRT PSI processing system (Sec. 2.1), the final PS points for each dataset were obtained. The graph in Fig. 4 brings a graphical representation of the processing datasets as the new images are obtained. Each processing dataset has 29 images that the time range is about one year. In principle, the final PS points derived from these 32 datasets were diverse. To be more specific, Fig. 5 illustrate PS points of three classes from the 29th (time period [06-Apr-2010 13-Mar-2011]) and 31st (time period [11-Jun-2010 04-Apr-2011]) processing datasets, implying green PS points were still highly coherent in both sequent processing datasets. The red PS points became extinct whereas the blue PS points emerged at certain moment.

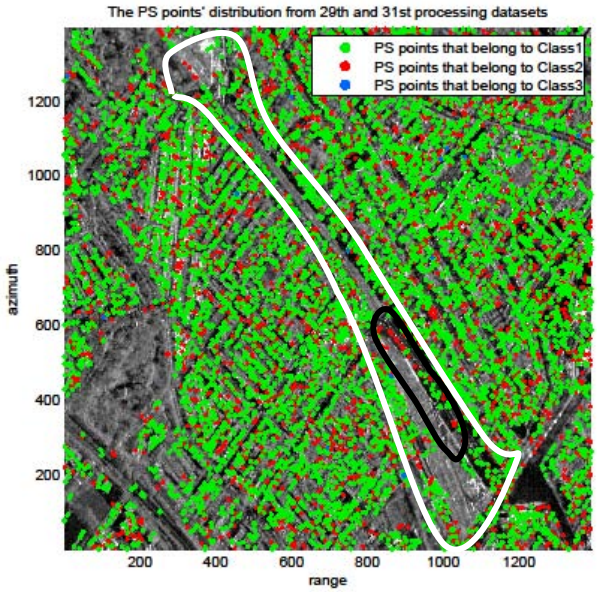

Figure 5. An example for the distribution of PS points from two different processing datasets. The 29th and 31st processing datasets are corresponding to 29th and 31st processing datasets respectively in Fig. 4. The green PS points are stable and coherent which belong to Class1. The red PS points disappeared in the 31st processing dataset which were stable in the 29th processing dataset. The blue PS points are new-born potential PS points in the 31st processing dataset. The white line covers a tunnel

construction area. A number of PS points in black circle disappeared due to this construction.

It is noted that owing to the difference between each distribution of STC histogram, the threshold for STC should be set specifically. The trade-off between the quality and quantity for the final PS points is concerned in the meantime. Fig. 6 illustrates an example for the distribution of STC histogram in four processing datasets. These four datasets are selected randomly from the 32 processing datasets. The red dashed line in each graph is the corresponding threshold value for STC. The values that are on the right side of the red dashed line are rejected. Consequently, we obtained 85% reliable PS points from each PS points' datasets.

On the basis of our classification criteria for PS points, the PS points were divided into three classes and tracked. With the purpose of verifying the real location of scatterers, the comparison of PS locations with detailed topographic maps will be followed by field inspection. The next subsection presents the results of PS points' deformation time series and amplitude for the three classes.

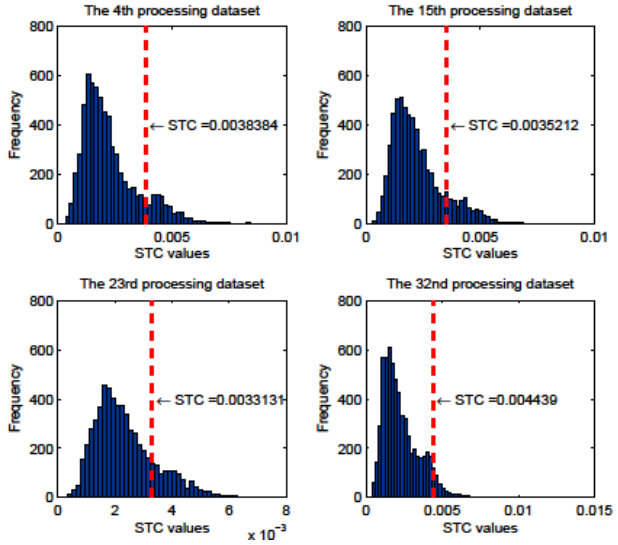

Figure 6. An example for the distribution of STC in four processing datasets. The red dashed line is the STC threshold, the values that are lower than the STC threshold are accepted. 85% reliable PS points from each PS points' datasets are obtained.

3.3 Results

In our case study, all the estimated linear deformation velocities in Line of Sight (LOS) for PS points in the 32 processing datasets were not really obvious. The PS points' deformation velocity from the 32nd processing dataset (corresponding time period is [22nd-06-2010, 15th-04-2011]) is depicted in Fig. 7 as an example. It is shown that most of PS points had slight deformation velocity in LOS direction. Most of the PS points around the tunnel construction area (in white polygon), also had slight subsiding trend.

On the grounds of classification criteria for PS points and the testing approach as stated before, the final PS points for three classes were classified and archived. Here we selected three PS points near the ongoing tunnel construction area to illustrate the deformation time series for the three classes PS points. Their locations are marked with red, green and blue in Fig. 8. Three PS points are named as *PS(II)*, *PS(I)* and *PS(III)* separately.

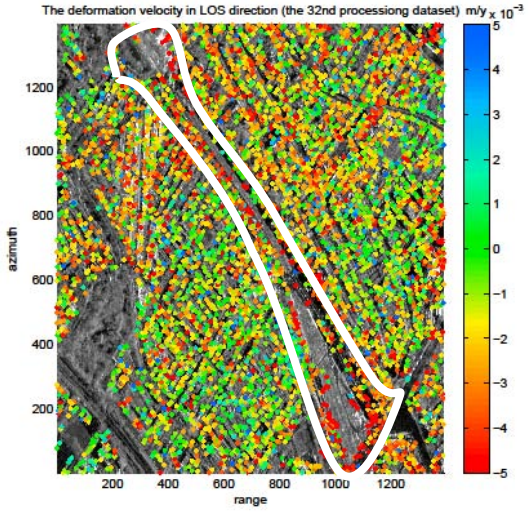

Figure 7. The PS points' linear deformation velocity in LOS direction obtained from the 32nd processing dataset. The white line covers the tunnel construction area.

Figure 8. The locations for three PS points. The white rectangle is the area of ongoing tunnel construction. This tunnel construction started on 15th August 2009 and will be completed in 2017

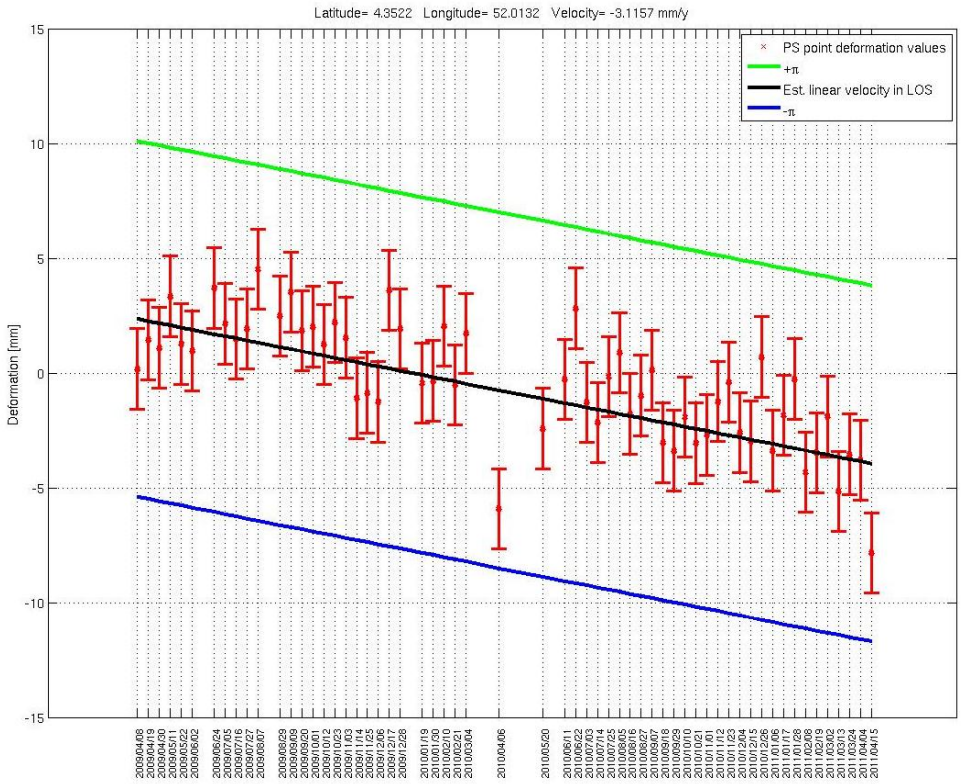

Figure 9. The deformation time series of PS point (I), belonging to Class1 PS points

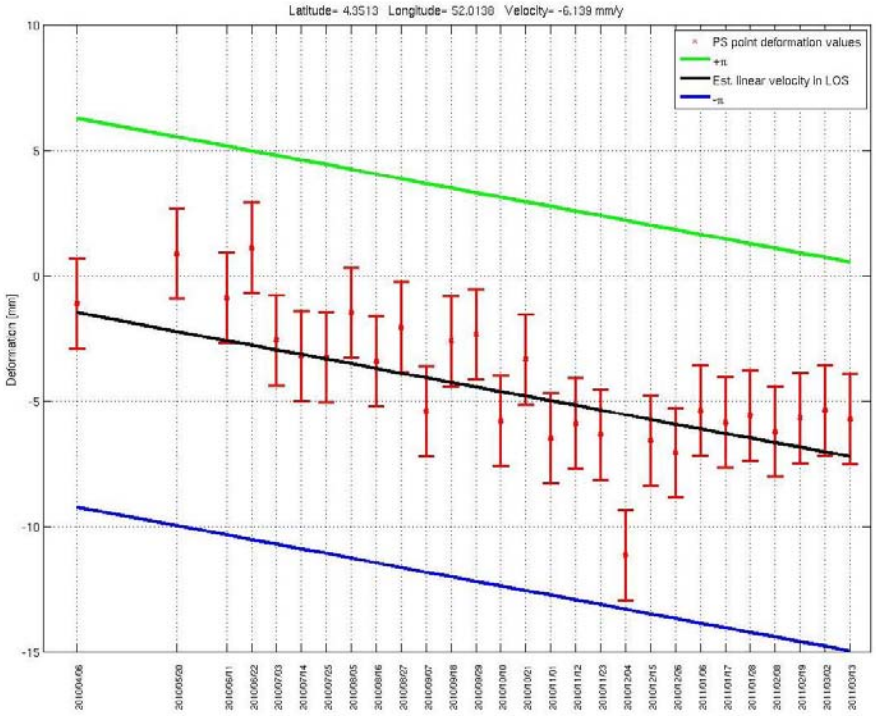

Figure 10. The deformation time series of PS point (II), belonging to Class2 PS points

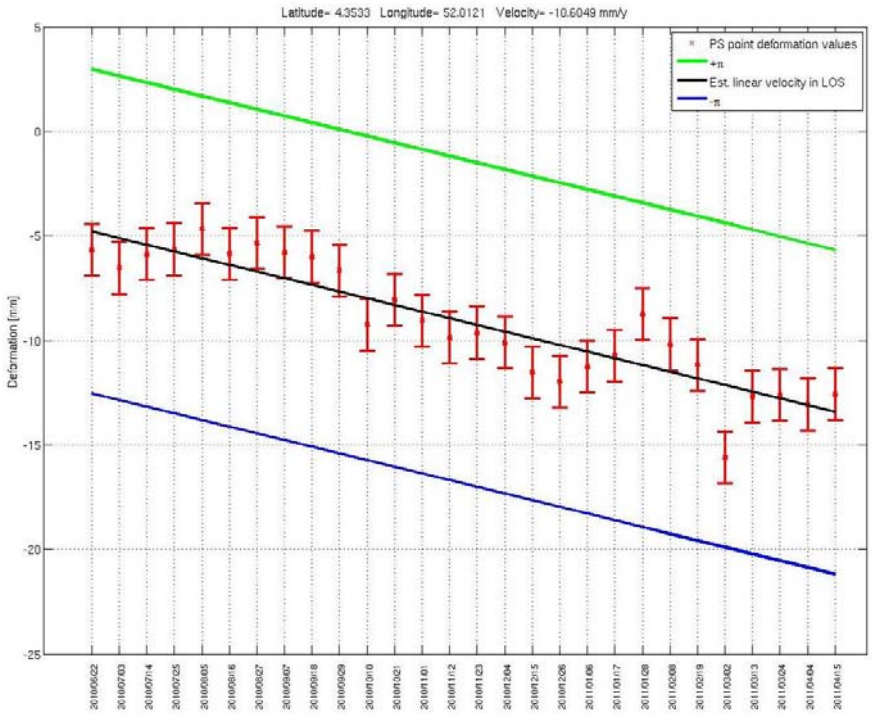

Figure 11. The deformation time series of PS point (III), belonging to Class3 PS points

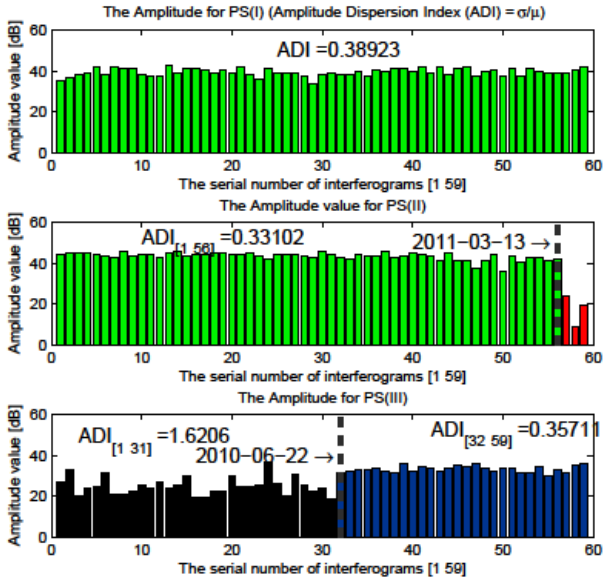

Figure 12. The amplitude of PS(I), PS(II) and PS(III) for 59 generated interferograms. The x-axis denotes the sequential number of the interferograms, the corresponding amplitude value [dB] is depicted on y-axis.

In the plots of Fig. 9, Fig. 10 and Fig. 11, the red dots with error bar are estimated deformation following with its standard deviation. Besides the fitted linear deformation velocity in black, two potential velocity lines in green (+π) and blue (-π) caused by ambiguity are plotted. Fig. 9 depicts the deformation in whole time series of the PS point (*PS(I)*) in a building (situates at 52.0132º*N*, 4.3522º*E*). This PS point belongs to Class1 PS points that keep coherent in whole time history. The PS point (*PS(II)*) (52.0138º*N*, 4.3513º*E*) on the windmill kept stable till 13th-03-2011 and disappeared in 24th-03-2011 due to the influence of digging train tunnel. Fig. 10 shows the deformation time series of this point in the 29th processing dataset which disappeared in the 30th processing dataset. In Fig. 11, we show the deformation time series for a new-born PS point (*PS(III)*) (situates at 52.0121º*N*, 4.3533º*E*, belonging to Class3 PS points).

Meanwhile in order to demonstrate the stability of these three PS points, we show their amplitude values of each 59 interferograms in Fig. 12. In the top plot, the amplitude value of *PS(I)* fluctuated slightly. The middle plot shows the amplitude of *PS(II)*. The amplitude of *PS(II)* in middle plot were stable till 13th-Mar-2011. After that moment, the last three amplitude values were lower than before. It demonstrates that the PS point vanished caused by the tunnel construction. The bottom plot shows the amplitude of *PS(III)*. It is obvious that the amplitude

values were quite different till 22nd-June-2010. There is a statistical relationship between amplitude stability and phase stability. The low Amplitude Dispersion Index (ADI) value it has, the more stable its phase is in time [11].

4. CONCLUSIONS

In this study we presented the Near Real-time deformation monitoring system based on PSI. A testing approach is applied so that the PS points and residual errors can be discriminated, which is able to reduce the influence from type-I/type-II errors. The deformation behavior for all available PS points can be tracked in accordance with our testing approach consequently. The initial results on the Delft test site are encouraging and support future development, leading to systematic updates and early warning possibilities in case of abnormal deformation.

5. ACKNOWLEDGMENT

This study was supported by Delft University of Technology, and the authors appreciate that German Aerospace Center (DLR) for providing the TerraSAR-X data for processing, and also thanks to Jet Propulsion Laboratory where can free download DEM data.

REFERENCES

1. Hanssen, R.F. (2001). *Radar Interferometry: Data Interpretation and Error Analysis.* Kluwer Academic Publishers, Dordercht, the Netherlands.
2. Ferretti, A., Prati, C. & Rocca, F. (2000*). Nonlinear subsidence rate estimation using permanent scatterers in differential SAR Interferometry*. IEEE Trans. Geoscience Remote Sensing. 38(5), 2202-2212.
3. Ferretti, A., Prati, C. & Rocca, F. (2001). *Permanent scatterers in SAR Interferometry.* IEEE Trans. Geosci. Remote Sensing. 39(1), 8-20.
4. Marinkovic, P., F. van Leijen, G. Ketelaar & R. Hanssen (2006). *Recursive persistent scatterer interferometry*. Fringe 2005 Workshop.
5. Hanssen, R.F. (2004). *Stochastic modeling of time series radar interferometry*. In Proceedings IGARSS 2004, pages cdrom.
6. Teunissen, P.J.G., Simons, D.G., & Tiberius, C.C.J.M. (2005). *Probability and observation theory*. Delft University Press.
7. Perissin, D., Ferretti, A. et al (2008). *Repeat-pass SAR interferometry with partially coherenct targets.* Fring 2007 Workshop.
8. Mróz, M & Mleczko, M. (2008). *Potential of TerraSAR-X StripMap data in early and rapid agricultural crops mapping*, Proceedings of the 2008 MARS Annual Conference "Geomatics in support of the CAP" Ljubljana, Slovenia 3-5 December 2008.
9. Harant, O., Fallourd, R. et al (2009). *Preliminary TerraSAR-X observation for temperate glaciers on the Chamonix Mont Blanc test site.* IGARSS 2009.
10. Gernhard, S., Adam, N., Eineder, M. & Bamler, R. (2010). *Potential of very high resolution SAR for persistent scatterer interferometry in urban areas.* Annals of GIS, Vol. 16, No. 2, June 2010, 103-111.
11. Hooper, A.J. Segall, P. & Zebker, H. (2007). *Persistent scatterer interferometric synthetic aperture radar for crustal deformation analysis, with application to volcán alcedo, galápagos*. J. Geophys. Res, 112(B07407).